Viable Alternative to N719 for Dye-Sensitized Solar Cells

Yali Sun, Anthony C. Onicha, Mykhaylo Myahkostupov, and Felix N. Castellano*

Center for Photochemical Sciences and Department of Chemistry, Bowling Green State University, Bowling Green, Ohio 43403

ABSTRACT A new synthetically facile heteroleptic ruthenium(II) sensitizer $(NBu_4)[Ru(4,7\text{-dpp})(dcbpyH)(NCS)_2]$, coded as **YS5**, where NBu_4 is tetrabutylammonium, 4,7-dpp is 4,7-diphenyl-1,10-phenanthroline, and dcbpyH is the singly deprotonated surface anchoring derivative of 4,4′-dicarboxy-2,2′-bipyridine ($dcbpyH_2$), was designed, synthesized, and incorporated into regenerative mesoscopic titania-based dye-sensitized solar cells. The sensitizer has characteristic broad, high extinction coefficient MLCT bands spanning the visible spectrum. The compound was fully characterized by 1D and 2D ^{1}H NMR, MALDI-TOF-MS, UV−vis, photoluminescence, Raman, IR, and electrochemistry. **YS5** exhibits strong visible absorption properties with a molar extinction coefficient of 1.71×10^4 M^{-1} cm^{-1} at its 522 nm maximum. In operational liquid junction-based DSSCs under simulated AM 1.5G one-sun excitation (100 mW/cm^2), the photovoltaic performance of **YS5** compares almost equally against the current benchmark sensitizer **N719** in side-by-side comparisons, producing a power conversion efficiency of 6.05% with a maximum IPCE of 65% at 540 nm. The data presented in this manuscript strongly suggest that **YS5** is indeed a viable sensitizer for nanocrystalline TiO_2-based DSSCs, seemingly poised for widespread adaptation.

KEYWORDS: dye-sensitized solar cell • heteroleptic Ru^{II} sensitizer • metal-to-ligand charge transfer (MLCT) absorption • mesoscopic TiO_2 film • average photovoltaic performance parameters • power conversion efficiency.

INTRODUCTION

Dye-sensitized solar cells (DSSCs) have attracted considerable interest over the past two decades because of their low cost and facile fabrication in comparison to conventional photovoltaics (1−10). A typical DSSC consists of a nanocrystalline TiO_2 photoanode deposited on a transparent conducting glass substrate and sensitized to the visible spectrum by an appropriate covalently attached dye sensitizer, a cathode composed of a thin layer of platinum metal on transparent conducting glass, and a hole-transporting material placed in between the anode and the cathode. Upon photoexcitation, the sensitizer molecule undergoes a thermodynamically favorable electron injection into the conduction band of TiO_2, from where the charge is transported to the conducting glass substrate. The collected electron is then relayed through the external circuit to the cathode. The oxidized sensitizer is sequentially reduced/regenerated by the redox mediator, typically an iodide/triiodide (I^-/I_3^-) couple, which in turn recovers an electron from the cathode. It has been recently suggested that this regeneration step does not produce the sensitizer in the same environment that was initially photoexcited, but instead is succeeded by a slow cation transfer process eventually regenerating the initial sensitizer in its original environment (11). A more detailed study revealed an underlying Stark effect, wherein the electron injection into the conduction band of the nanocrystalline TiO_2 created an electric field resulting in the perturbation of the metal-to-ligand charge transfer (MLCT) electronic transitions of Ru(II) compounds anchored to the same TiO_2 surface (12). Thus, fundamental contributions in this area continue to emerge further exemplifying the need for close examination of new dye sensitizers. Although the nature of the titania, conductive substrates, electrolytes, redox mediator, and fabrication techniques are of key importance, the sensitizer at the heart of the device remains the major functional component. In view of net power conversion efficiency, stability to extended light-soaking, and compatibility with diverse electrolyte compositions, ruthenium(II) polypyridyl complexes with low energy metal-to-ligand charge transfer transitions presently surpass all other dyes in operational DSSCs (13, 14). The current trend in Ru(II) sensitizer engineering lies in the development of new chromophores with higher molar extinction coefficients and broader spectral response to achieve improved light harvesting. If these strategies realize success, the thickness of the titania film can be substantially reduced, thereby shortening electron transport distances and, thus, suppressing the underlying electron losses and increasing the overall device efficiencies (15, 16). In this regard, a number of ruthenium(II) sensitizers have been prepared, including molecules known as Z907, Z910, K19, K8, and C104 (17−22), along with a rather intriguing cyclometalated ruthenium sensitizer (14) strategically lacking the NCS^- ancillary ligands. Despite all these efforts, the highest NREL-certified devices are liquid junction cells based on the benchmark **N719** (Chart 1) and the so-called "black dye" complexes, producing 11.04 and 10.4% power conversion efficiencies under simulated AM 1.5G irradiation conditions, respectively (15, 23).

* Corresponding author. E-mail. castell@bgsu.edu. Phone: (419) 372-7513. Fax: (419) 372-9809.
Received for review April 06, 2010 and accepted June 07, 2010

DOI: 10.1021/am100311m

Chart 1. Structures of the Ru(II) Dye Sensitizers

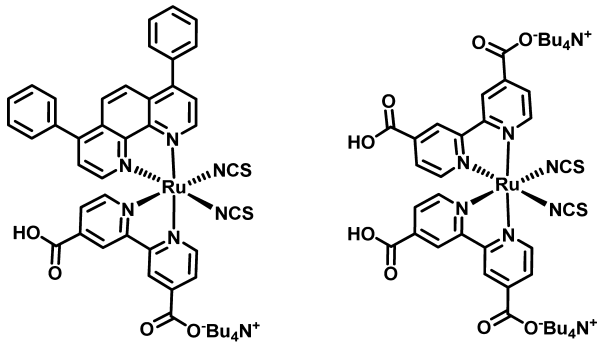

YS5 N719

Here we report a synthetically facile heteroleptic Ru(II) sensitizer with the molecular formula $(NBu_4)[Ru(4,7\text{-dpp})(dcbpyH)(NCS)_2]$, represented as **YS5**, where NBu_4 is tetrabutylammonium, 4,7-dpp is 4,7-diphenyl-1,10-phenanthroline, and dcbpyH is the singly deprotonated surface anchoring derivative of 4,4′-dicarboxy-2,2′-bipyridine ($dcbpyH_2$). The commercial availability of the 4,7-dpp ligand makes it rather attractive as a subunit for Ru^{II}-based sensitizers because it precludes lengthy heterocyclic ligand preparation and produces intense MLCT absorptions at wavelengths above 400 nm (24). Under the employed experimental conditions, the DSSCs using **YS5** as the sensitizer in combination with a 13 μm thick transparent mesoscopic layer and a 5 μm thick scattering layer of TiO_2 produced an efficiency of 6.05 ± 0.52 % with open-circuit voltage (V_{OC}) of 749 ± 16 mV, short-circuit current density (J_{SC}) of 14.52 ± 0.85 mA/cm^2 and fill factor (FF) of 55.7 ± 4.1 %. The values cited above are given for the average operational **YS5** device, as we only present data where critical solar cell parameters were measured across 6 parallel devices. We believe that this is a rational approach for making quantitative comparisons between structurally different dyes and device assemblies routinely produced in the research laboratory, because record-achieving DSSC devices are rarely realized.

EXPERIMENTAL SECTION

General. Dichloro(*p*-cymene)ruthenium(II) dimer, tetrabutylammonium hydroxide (TBAOH), ammonium thiocyanate (NH_4NCS), lithium iodide, guanidine thiocyanate, 4-*tert*-butylpyridine, titanium(IV) isopropoxide, hydroxypropyl cellulose (HPC), dimethylformamide (DMF), and tetrabutylammonium hexafluorophosphate ($TBAPF_6$) were purchased from Aldrich Chemical Co. 4,7-Diphenyl-1,10-phenanthroline and iodine were purchased from GFS Chemicals Incorporated and Alfa Aesar, respectively, and were used as received. Deionized water was obtained using a Barnstead Nanopure System. All other solvents were reagent grade and used without further purification. The syntheses of 4,4′-dicarboxy-2,2′-bipyridine ($dcbpyH_2$) (25) and 1-*n*-propyl-3-methylimidazolium iodide (PMII) (26) were carried out according to published procedures. The synthesis of $[Ru(4,7\text{-dpp})(dcbpyH_2)(NCS)_2]$ (**YS4**) was adapted from the well-known published one-pot procedure developed for heteroleptic polypyridyl ruthenium(II) complexes using $[Ru(p\text{-cymene})Cl_2]_2$ as the starting material (27). $(NBu_4)[Ru(4,7\text{-dpp})(dcbpyH)(NCS)_2]$ (**YS5**), the singly deprotonated species of **YS4**, was obtained by titrating a basic aqueous solution of **YS4** with 0.02 M nitric acid to pH 4.3. The structural characterization of the new complexes was confirmed by ^1H and ^{13}C NMR, MALDI-TOF mass spectrometry, ATR-FTIR, and Raman spectroscopy.

Characterization, Physical Measurements, and Instrumentation. The ^1H NMR and ^{13}C NMR spectra were recorded on a Bruker Avance 300 (300 MHz) while the $^1H-^1H$ COSY NMR, HSQC and HMBC spectra were recorded on a Bruker Avance III 500 (500 MHz) spectrometer. All chemical shifts were referenced to the residual solvent signals and splitting patterns were designated as s (singlet), d (doublet), t (triplet), q (quartet), m (multiplet), and quint (quintet). MALDI-TOF mass spectra were measured by a Bruker-Daltonics Omniflex spectrometer. The ATR-FTIR spectra were measured as neat solids or on TiO_2 films on a ThermoNicolet IR 200 spectrometer by using an attenuated total reflectance (ATR) assembly at a resolution of 8 cm^{-1}. Resonance Raman spectra were obtained using a Renishaw inVia Raman Microscope equipped with a HeCd laser providing 442 nm output. The same microscope system was utilized to measure the Raman spectra of "naked" titania materials, however, in this case the excitation was afforded by a 785 nm laser diode. All photophysical experiments were conducted using 1 cm^2 anaerobic quartz fluorimeter cells (Starna Cells, Inc.). Steady-state UV−vis electronic absorption spectra in solution were measured on a Shimadzu UV-3600 spectrophotometer with a resolution of 0.2 nm. Steady-state photoluminescence spectra were measured with a single photon counting spectrofluorimeter from Edinburgh Analytical Instruments (FL/FS 900) and excitation was provided using a 450 W Xe lamp. All samples were optically dilute solutions prepared in analytical grade solvents. Photoluminescence lifetimes were obtained by using a nitrogen-pumped broadband dye laser as the excitation source (PTI GL-3300 Nitrogen laser, PTI GL-301 dye laser, C500 dye) and a transient detection system described previously (28). All samples were deaerated with argon gas for at least 20 min prior to lifetime measurements. The excited-state lifetimes were obtained from the first-order decay fit of single wavelength emission transients in Origin 8.0 software with goodness of -fit determined by visual inspection of the residuals. Electrochemical data were obtained using a BAS Epsilon electrochemistry workstation with a conventional three-electrode arrangement. Cyclic voltammetry measurements were carried out in deaerated DMF solution containing 0.1 M tetrabutylammonium hexafluorophosphate as the supporting electrolyte, a platinum microdisk (1.6 mm dia.) working electrode, a platinum wire auxiliary electrode and a Ag/AgCl (3 M NaCl) reference electrode (BAS model MF-2079), respectively. Measurements were conducted in ca. 1 mM electroactive substrate under an inert gas atmosphere with a scan rate of 100 mV/s and ferrocenium/ferrocene was used as internal standard. For all measurements, potentials were recorded vs. the ferrocenium/ferrocene (Fc^+/Fc) internal standard, and finally were converted to $E_{1/2}$ vs. the normal hydrogen electrode (NHE) using $E_{1/2}(Fc^+/Fc^0) = +0.72$ V vs NHE (22, 29). The thickness of TiO_2 films was determined by a KLA-Tencor Alpha-Step IQ Surface Profiler. Incident photon-to-current conversion efficiency (IPCE) measurements were carried out using a system from PV Measurements, Inc., equipped with a Xe arc lamp and calibrated with a silicon reference photodiode. Current−voltage characteristics were measured on an I−V data acquisition system (PV Measurements, Inc.) equipped with a small area solar simulator (AM 1.5 Global) and an NREL-certified silicon reference solar cell (PVM 274, ISO tracking number 1374, NREL) for calibrating the intensity of the simulated sunlight to 100 mW/cm^2, with the measured photocurrent being within 2 % of its calibration value. Photocurrent density (J_{SC}) values directly measured using $I-V$ curves were typically 10−15 % larger than those estimated from the integrated EQE (IPCE) spectra. Estimation of J_{SC} was performed by the $I-V$ software (PV Measurements Inc.) according to the ASTM standard E1021. The sandwiched solar cells were

Scheme 1. Synthetic Route Used for the Preparation of YS5

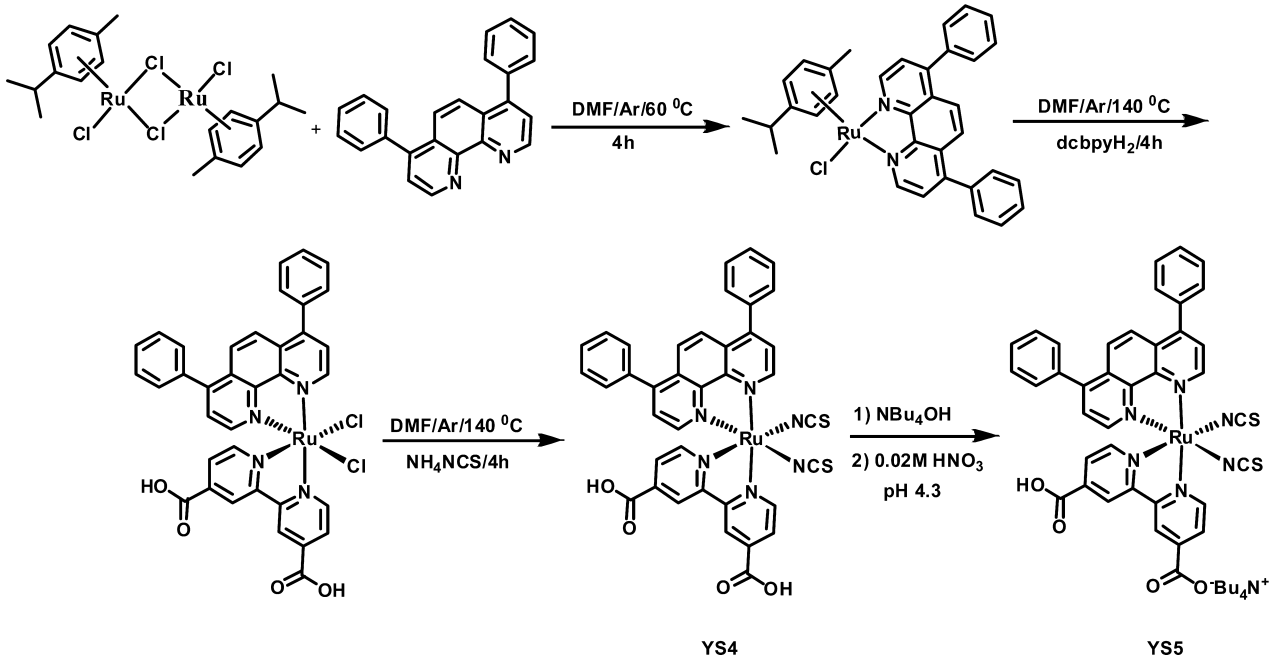

illuminated directly through the transparent conductive glass support containing the TiO_2 photoanode. The photovoltaic performance, including photocurrent density, photovoltage, power conversion efficiency, and incident photon-to-current conversion efficiency (IPCE) are reported herein as overall yields that were not corrected for losses due to light absorption and reflection by the conductive glass support.

Synthesis and Characterization. ***[Ru(4,7-dpp)(dcbpyH$_2$)(NCS)$_2$] (YS4).*** The synthesis of **YS4** was accomplished through adaptation of the established one-pot procedure developed for heteroleptic polypyridyl ruthenium(II) complexes using [$RuCl_2$(*p*-cymene)]$_2$ as the starting material as shown in Scheme 1 (27). 4,7-Diphenyl-1,10-phenanthroline (4,7-dpp) (179.5 mg, 0.54 mmol) and dichloro(*p*-cymene)ruthenium(II) dimer (163.5 mg, 0.27 mmol) in 50 mL DMF were heated at 60 °C for 4 h under argon with continuous stirring in the dark. Subsequently, 4,4′-dicarboxy-2,2′-bipyridine (132 mg, 0.54 mmol) was added and the reaction mixture was heated to 140 °C for 4 h. To the resulting dark green solution was added an excess amount of NH_4NCS (615 mg, 8.1 mmol) and the reaction mixture was maintained at 140 °C for another 4 h. After cooling down to RT, most of the solvent was removed on a rotary evaporator under vacuum and deionized water (200 mL) was added, producing a precipitate. The purple solid was filtered off, washed with water and diethyl ether, and dried under a vacuum. The crude product was dissolved in basic methanol containing tetrabutylammonium hydroxide and further purified over Sephadex LH-20 with methanol as eluent. The main band was collected, concentrated and precipitated with dilute sulfuric acid to pH ~1.2 to obtain the pure title compound (325 mg, 76% yield). MALDI-MS (TOF): 794.22 ($[M]^+$), 736.22 ($[M - NCS]^+$). ^{1}H NMR (500 MHz, CD_3OD + TBAOH, aromatic region) δ: 9.80 (d, J = 5.0 Hz, 1H, H^2), 9.61 (d, J = 5.5 Hz, 1H, $H^{e'}$), 9.05 (d, J = 1.5 Hz, 1H, $H^{b'}$), 8.86 (d, J = 1.5 Hz, 1H, H^b), 8.25 (dd, J_1 = 1.5 Hz, J_2 = 5.5 Hz, 1H, $H^{d'}$), 8.21 (d, J = 9.5 Hz, 1H, H^5), 8.14 (d, J = 5.5 Hz, 1H, H^3), 8.09 (d, J = 9.5 Hz, 1H, H^6), 7.99 (d, J = 5.5 Hz, 1H, H^9), 7.80 (m, 2H, phenyl), 7.61 − 7.70 (m, 4H, phenyl + H^e), 7.54 (m, 5H, phenyl), 7.49 (d, J = 6 Hz, 1H, H^8), 7.47 (dd, J_1 = 1.5 Hz, J_2 = 6 Hz, 1H, H^d). ^{13}C NMR (125 MHz, CD_3OD + TBAOH, aromatic region) δ: 170.61 (C′═O), 170.35 (C═O), 160.47 (C^a), 159.45 ($C^{a'}$), 154.37 (C^2), 154.32 ($C^{e'}$), 153.21 (C^9), 153.08 (C^e), 151.44 (C^{13}), 150.30 (C^{11}), 149.44 (C^4), 148.75 (C^7), 147.62 ($C^{c'}$), 146.92 (C^c), 137.71 (C^{19}), 137.36 (C^{25}), 134.57 (C^{NCS}), 134.33 (C^{NCS}), 131.19 (phenyl), 130.92 (phenyl), 130.58 (phenyl), 130.43 (phenyl), 130.26 (phenyl), 130.09 (phenyl), 129.60 (C^{10}), 129.50 (C^{12}), 127.06 ($C^{d'}$), 127.03 (C^3), 126.81 (C^5), 126.69 (C^6), 126.39 (C^8), 126.32 (C^d), 123.71 ($C^{b'}$), 123.48 (C^b).

(NBu$_4$)[Ru(4,7-dpp)(dcbpyH)(NCS)$_2$] (YS5). Sixty milligrams of **YS4** was completely dissolved in 20 mL of a tetrabutylammonium hydroxide (TBAOH) aqueous solution in a 50 mL Erlenmeyer flask. The pH of this solution was adjusted to 4.3 by the dropwise addition of 0.02 M nitric acid, at which point most of the complex precipitated out. The suspension was stirred at room temperature for 3 h, and afterwards it was left in a freezer at approximately −20 °C overnight. When the flask was warmed back to room temperature, the final solid product was collected on a sintered glass crucible. ^{1}H NMR (300 MHz, CD_3OD) δ: 9.82 (d, J = 5.4 Hz, 1H), 9.71 (d, J = 6 Hz, 1H), 9.08 (s, 1H), 8.90 (s, 1H), 8.31 (dd, J_1 = 1.5 Hz, J_2 = 6 Hz, 1H), 8.22 (d, J = 9.3 Hz, 1H), 8.16 (d, J = 5.7 Hz, 1H), 8.09 (d, J = 9.6 Hz, 1H), 7.99 (d, J = 5.4 Hz, 1H), 7.81 (dd, J_1 = 1.5 Hz, J_2 = 5.4 Hz, 2H), 7.75 (d, J = 6 Hz, 1H), 7.71−7.62 (m, 3H), 7.55−7.51 (m, 6H), 7.48 (d, J = 5.7 Hz, 1H), 3.24 (m, 8H), 1.67 (m, 8H), 1.40 (quint, J = 7.5 Hz, 8H), 1.01 (t, J = 7.2 Hz, 12H).

Preparation of Nanocrystalline TiO_2 Electrode and Transparent Platinum Cathode. The sol−gel synthesis of the colloidal TiO_2 paste is described in detail elsewhere (30, 31). The prepared TiO_2 paste was doctor-bladed onto the conductive glass substrate (Hartford Glass, TEC-15) to give the transparent layer of TiO_2 film with a typical thickness of 13 μm. The obtained nanoparticle film was then dried at 125 °C for 6 min and a 5 μm thick scattering layer of mesoscopic TiO_2 (Solaronix, Ti-Nanoxide 300) was doctor-bladed on top of it. The resulting TiO_2 films were subsequently annealed for 30 min at 500 °C under an oxygen flow in a tube furnace with ramped heating control of 5 °C per minute. Raman spectroscopy of the neat titania film (λ_{ex} = 785 nm) confirmed that only the anatase polymorph was present (see Supporting Information). Upon being cooled to 80 °C, TiO_2 electrodes were immersed in 0.5 mM sensitizer solution in acetonitrile/*tert*-butanol (50:50 v/v %) for 24 h at RT. After completion of the film sensitization, the TiO_2 electrodes were withdrawn from the dye solution, rinsed with acetonitrile, dried under an argon stream, and stored until

use. Transparent platinum-coated FTO cathodes were prepared as described elsewhere (31).

Sandwiched Solar-Cell Assembly. The active device area of the sensitized TiO_2 photoanode was adjusted to 0.25 cm^2. Stretched Parafilm-M was used as a spacer between the photoanode and the platinum counter electrode. The typical thickness of the spacer was 30 μm. A few drops of the redox electrolyte were placed on top of the active electrode area and a platinized FTO-glass counter electrode was placed on top. The electrodes were then sealed together using binder clips. For these studies, the redox electrolyte solution consisted of 0.1 M LiI, 0.05 M I_2, 0.6 M 1-*n*-propyl-3-methylimidazolium iodide (PMII), 0.5 M 4-*tert*-butylpyridine (4-^{t}Bupy), and 0.1 M guanidine thiocyanate (guan. thio.) in anhydrous acetonitrile (30).

RESULTS AND DISCUSSION

Synthesis. The use of π-conjugated acceptor ligands have been shown to enhance the molar extinction coefficients of the ruthenium(II) polypyridyl complexes used as sensitizers in DSSCs (14, 19−22, 32−37). As previously reported, the substitution of a phenyl group in the proper positions of a polypyridyl ligand such as bipyridine or phenanthroline in ruthenium(II) complexes enhances the molar extinction coefficients in the MLCT transitions (38−40). The incorporation of phenyl group in 4,7-substituted positions of phenanthroline also greatly prolongs the excited state lifetime (40, 41). The commercially available 4,7-dpp ligand, where dpp is 4,7-diphenyl-1,10-phenanthroline, is an attractive subunit for Ru^{II}-based sensitizers since it precludes lengthy heterocyclic ligand preparation and produces intense MLCT absorptions at wavelengths above 400 nm. In addition, the introduction of two aromatic phenyl groups on the 4,7-positions of phenanthroline provides increased hydrophobicity for the sensitizers, which may assist in maintaining long-term device stability.

The degree of deprotonation of the $dcbpyH_2$ ligand of the ruthenium(II) sensitizers is known to greatly influence the properties of these chromophores (15, 42, 43). These include the absorption maxima and molar extinction coefficients, photophysical properties such as emission maxima, quantum yield, and excited state lifetimes, in addition to the redox properties and ultimately the photovoltaic performance of the operational sandwiched solar cells (15, 42, 43). The benchmark chromophore **N719** is the doubly deprotonated species of **N3**. It possesses a superior photovoltaic performance than the fully protonated **N3** in addition to the fully deprotonated species (42). Hence, for comparison, **YS5**, the singly deprotonated derivative of **YS4**, was thoroughly investigated herein as a sensitizer in DSSCs.

Details of the synthetic approach adopted for the preparation of the heteroleptic complex **YS5** are presented in Scheme 1. The assignments for the ^1H and ^{13}C for **YS4** in deuterated methanol with TBAOH are discussed in the Supporting Information. By comparing the integration of the proton peaks for tetrabutylammonium in the aliphatic region with the integration of the proton peaks in the aromatic region, it was determined that only one of the carboxylic groups of **YS5** was indeed deprotonated, confirming the proposed structure.

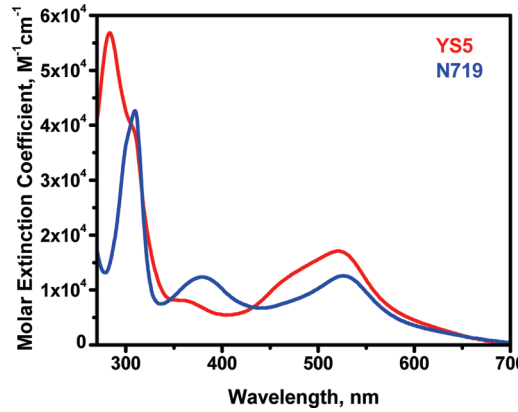

FIGURE 1. Ground-state absorption spectra of YS5 (red) and N719 (blue) at RT in DMF solution.

Absorption and Photoluminescence. The electronic absorption spectra of **YS5** and **N719** were recorded at room temperature in aerated DMF solution (Figure 1). Both complexes exhibit broad and intense MLCT absorption bands throughout the visible region of the spectrum (400−700 nm) characteristic of many other ruthenium(II) polypyridyl complexes which can be assigned to electronic transitions from the Ru^{II} based t_{2g} orbital to the ligand based π^* orbitals (Ru > 610 > 4,7-dpp and Ru → dcbpyH). The intense absorption bands in the UV region around 310 and 280 nm are due to the intraligand $\pi-\pi^*$ transitions of dcbpyH and 4,7-dpp ligands, respectively. The lower-energy absorption around 310 nm is assigned to the dcbpyH ligand $\pi-\pi^*$ transition because the electron withdrawing nature of the carboxylic groups lowers the energy of the π^* orbital of the bipyridine ligand relative to that of the more donating 4,7-dpp ligand.

As found in related 4,7-dpp-containing Ru^{II} complexes (24), the molar extinction coefficient of the MLCT absorption bands in **YS5** is greater than that of **N719** at all wavelengths above 430 nm (Figure 1, Table 1). The molar extinction coefficient of **YS5** at its maximum (522 nm) is 1.71×10^4 M^{-1} cm^{-1}, precisely 4500 M^{-1} cm^{-1} larger than that of N719 (1.26×10^4 M^{-1} cm^{-1}). The heteroleptic nature of **YS5** produces multiple MLCT transitions in the visible, i.e., Ru → 4,7-dpp and Ru → dcbpyH, thus enhancing the oscillator strength in the blue and green portions of the spectrum relative to **N719**. As a result, improved light absorption cross-sections at higher energy are indeed realized in **YS5**.

Steady-state emission spectra were measured in aerated DMF at room temperature upon 510 nm excitation in conjunction with a 550 nm long pass filter placed in the emission path. For **YS5,** a weak photoluminescence was observed with a corrected maximum centered at ~801 nm. The excited state energy $E(0-0)$ was estimated to be at 681 nm, corresponding to 1.82 eV. The excited state lifetime in argon saturated DMF solution was determined to be 138 ns. Note that the excited state lifetime of **YS5** in DMF is enhanced with respect to **N3** (20 ns) (42) and **N719** (40 ns) (42) in aerated ethanol solution at RT. This is most definitely a result of the phenyl substituents in the 4,7-positions on the phenanthroline as discussed above (40, 41). The long excited

Table 1. Photophysical and Electrochemical Properties of YS5 and N719 in DMF Solution at RT[a]

	abs λ_{max} (nm) (ε ($\times 10^4$ M^{-1} cm^{-1}))							
sensitizer	$\pi-\pi^*$	$d\pi-\pi^*$	em. λ_{max} (nm)	E_{0-0} (eV)	τ (ns)	$E_{1/2}(S^+/S)^b$ (V vs NHE)	$E(S^+/S^*)$ (V vs NHE)	$E_{1/2}red^b$ (V vs NHE)
YS5	283 (5.68)	308 (3.95)	801	1.82	138	1.05	−0.77	−1.15,−1.55
	362 (0.81)	522 (1.71)						
N719	310 (4.26)	382 (1.24)	837	1.85	40[c]	1.14	−0.71	−1.15
		527 (1.26)						

[a] The electrochemical data were measured with platinum working electrode in deaerated DMF solution containing 0.1 M $TBAPF_6$ with a scan rate of 100 mV/s and ferrocenium/ferrocene (Fc^+/Fc) as an internal standard. [b] Determined by cyclic voltammetry and differential pulse voltammetry. [c] Measured in aerated ethanol solution.

state lifetime of **YS5** therefore provides a sufficient kinetic situation for the photoexcited sensitizer to inject electrons into the conduction band of TiO_2 from both ^{1}MLCT and ^{3}MLCT excited states, a process that for Ru^{II}-based dyes typically occurs on the femtoseconds time scale (44, 45). Complete photophysical and electrochemical data of **YS5** and **N719** are summarized in Table 1.

Electrochemistry. The cyclic voltammogram of **YS5** displays a quasi-reversible one-electron oxidation process at $E_{1/2} = +1.05$ V versus NHE for the $Ru^{III/II}$ wave, Figure S7. Two ligand reduction peaks are observed at −1.15 (reversible) and −1.55 V (quasi-reversible) versus NHE. The more positive reduction potential is assigned to dcbpyH due to the electron withdrawing COOH group being responsible for lowering the LUMO levels. The oxidation potential of the excited state was calculated by the following equation: $E(S^+/S^*) = E_{1/2}(S^+/S) - E(0-0)$ (22), where $E_{1/2}(S^+/S)$ is the ground state oxidation potential and $E(0-0)$ is the estimated HOMO−LUMO energy gap. The oxidation potential of the excited state of **YS5** (−0.77 V vs NHE) is more negative than the conduction band of the semiconductor ($E_{cb}(TiO_2) = -0.4$ V vs NHE) (46, 47), and its ground state oxidation potential (+1.05 V vs. NHE) is more positive than the redox mediator ($I^-/I_3^- = +0.4$ V vs. NHE) (46, 47). Evidently, the relative alignment of energy levels of all species involved in the photoaction cycle in DSSC provides sufficient thermodynamic driving force for both efficient electron injection from **YS5** excited state into the conduction band of TiO_2 (∼370 mV) in addition to subsequent regeneration of the oxidized sensitizer by the iodide/triiodide redox mediator (∼650 mV).

Photovoltaic Performance of DSSCs. For both studied sensitizers, incident photon-to-current conversion efficiency (IPCE) and *I*−*V* characteristics were measured under identical experimental conditions. At least six independent DSSC devices were measured in parallel to quantitatively investigate how reproducibly **YS5** performs as a sensitizer in DSSC applications. All critical solar cell parameters were therefore measured across six devices in parallel assembled following the identical procedure. DSSCs utilizing **N719** as the sensitizer were prepared and used as benchmarking controls in all photovoltaic experiments presented below.

On the basis of the absorption properties of **YS5** (Figure 1), this sensitizer is expected to sufficiently harvest a large portion of incident solar energy even when bound to a relatively thin semiconductor film. Presumably, the maximal photocurrent will be generated when the thickness of the TiO_2 film is smaller than the effective electron diffusion length, so that the recombination losses are minimized (48). However, in any particular case, the optimal thickness of a mesoscopic TiO_2 film often depends on the preparation methodology making it very difficult to predict and is generally revealed by exercising various experimental conditions. For example, it was recently shown that electron injection dynamics are sensitive to film properties related to nanoparticle size and crystallinity (49). Ultimately, the photovoltaic performance of the operating device will be governed by the interplay between several parameters including light harvesting efficiency (LHE), charge transport and collection, and dye regeneration kinetics. In principle, thinner TiO_2 films would provide lower bulk resistance and shorter charge transport pathways, thus improving the overall device efficiency, but infinite reduction of the film thickness will ultimately lead to a reduced number of bound sensitizer molecules and, consequently, to lower photocurrents. On the other hand, when thicker films are employed, more dye molecules will be adsorbed resulting in the enhancement of both IPCE and generated photocurrent. However, such loss mechanisms as charge recombination through different pathways are likely to become more pronounced in case of thicker TiO_2 films (48, 50). In general, as was shown in a number of studies for various TiO_2 morphologies, there exists a balance between the thickness of TiO_2 film, the chemical and photophysical properties of a given sensitizer, and the photovoltaic device efficiency (51−54). In the present study, by incorporating a 5 μm thick TiO_2 scattering layer in conjunction with a 13 μm thick transparent TiO_2 nanoparticle film, the devices based on both **N719** and **YS5** sensitizers yielded the best photovoltaic performance under all of our experimental conditions. These films therefore represent a compromise situation wherein reasonable light harvesting properties are achieved in films that remain prone to resistive losses due to a film thickness mandated by the sensitizers at the heart of this work.

Figure 2 presents averaged IPCE spectra for DSSC devices based on **YS5** and **N719** sensitizers bound to a 13 μm thick transparent TiO_2 electrode (no scattering layer was applied). Under identical conditions, the average IPCE response for **YS5**-based devices was very close to that of **N719**-based DSSCs across the whole visible region of the spectrum.

The IPCE spectral response for the **YS5** sensitizer at its maximum wavelength of 540 nm is 65%, as compared to

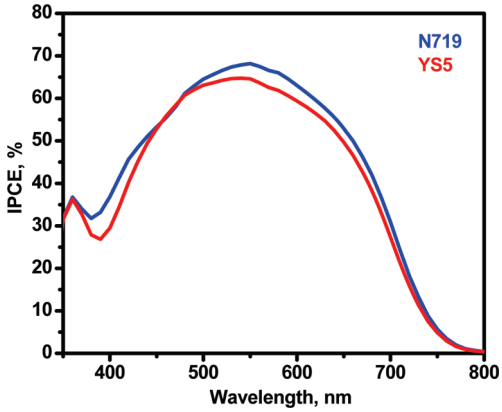

FIGURE 2. Averaged IPCE spectra for DSSCs based on YS5 (red) and N719 (blue) sensitizers bound to 13 μm thick transparent TiO_2 film electrodes.

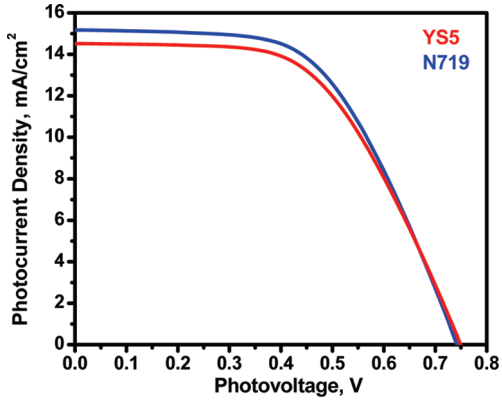

FIGURE 3. Average $I-V$ characteristics of DSSCs achieved in our laboratory based on YS5 (red) and N719 (blue) sensitizers bound to TiO_2 electrode comprised of a 13 μm thick transparent mesoscopic layer and a 5 μm thick scattering layer.

~68% for **N719** at its corresponding maximum of 550 nm. Over the spectral range of 350−800 nm, the integrated IPCE response exhibited by **YS5**-based devices was approximately 6.2% lower overall with respect to **N719**. In theory, the observed lower IPCE response would suggest slightly less efficient photocurrent generation of **YS5**-based devices with respect to ones based on **N719** and, as demonstrated below, indeed correlates well with the observed trends in the $I-V$ characteristics of the solar cells.

As shown in the $I-V$ curves (Figure 3), the average solar cell composed of a 13 μm thick transparent layer and a 5 μm thick scattering layer of TiO_2 film based on **YS5** produced photovoltaic performance with (averaged values) an overall power conversion efficiency (η) of 6.05 ± 0.52%, short-circuit current (J_{SC}) of 14.52 ± 0.85 mA/cm^2, open-circuit voltage (V_{OC}) of 749 ± 16 mV and fill factor (*FF*) of 55.7 ± 4.1%, whereas **N719**-based devices, fabricated and measured under identical conditions, displayed an average power conversion efficiency of 6.32 ± 0.41% with J_{SC} of 15.17 ± 0.45 mA/cm^2, V_{OC} of 741 ± 4 mV, and FF of 56.1 ± 3.2% (Table 2). In correlation with measured IPCE spectra (Figure 2), the **YS5**-based devices generated slightly lower photocurrent (~4.5%) as compared to **N719**, whereas both V_{OC} and FF were essentially the same within the experimental error. It is this difference in photocurrent that ultimately results in **YS5**-based devices being ~4.5% less efficient with respect to those based on **N719**. Even though the photovoltaic properties of **YS5** did not exceed those of **N719** in terms of power conversion efficiency, the observed differences are rather insignificant. As a result, **YS5** can be safely considered to be a viable alternative for DSSC utilization and most definitely outperforms a number of Ru^{II} dyes that have been developed over the past two decades (55).

Table 2. Averaged Photovoltaic Performance Parameters of DSSCs Based on YS5 Sensitizer As Compared to N719

sensitizer	V_{OC} (mV)	J_{SC} (mA/cm^2)	FF (%)	η (%)	$IPCE_{max}$
YS5	749 ± 16	14.52 ± 0.85	55.7 ± 4.1	6.05 ± 0.52	64.6 ± 1.2
N719	741 ± 4	15.17 ± 0.45	56.1 ± 3.2	6.32 ± 0.41	68.2 ± 1.4

The observed marginally inferior photovoltaic performance of **YS5** could be traced to several factors, but may be limited in part by the choice of redox mediator used in the present study. It is a common consensus that the iodide/triiodide redox couple is well-suited for Ru^{II} dyes such as **N3** or **N719** that possess similar electronic properties (56). On the other hand, as in the cases of other dyes, the same redox couple is not guaranteed to produce optimum results and, as a result, can cause such unwanted effects as retardation of electron injection, inefficient dye regeneration, and electron losses due to increased back electron transfer. The overall cumulative effect would result in DSSCs that are less efficient than those based on either **N3** or **N719**. Unfortunately, up to this moment in time, no other redox couple has been shown to outperform the above-mentioned corrosive iodide/triiodide mediator. Regardless, **YS5** indeed exhibits competitive photovoltaic behavior with respect to **N719** across a series of routinely fabricated liquid junction laboratory devices and we anticipate it to become one of the mainstream sensitizers for DSSCs based on nanocrystalline TiO_2.

CONCLUSION

In conclusion, a synthetically facile heteroleptic ruthenium(II) sensitizer (**YS5**) with broad spectral bandwidth and visible light absorption properties was designed, synthesized, and incorporated as the dye sensitizer in operational DSSCs. In our hands, **YS5** has been shown to statistically approach the benchmark **N719** chromophore in terms of photovoltaic performance across a series of routinely fabricated liquid junction laboratory devices. Under AM 1.5G one-sun illumination, the average DSSC device with **YS5** sensitizer composed of a 13 μm transparent layer and a 5 μm scattering layer of TiO_2 film with iodide/triiodide electrolyte produces an overall average power conversion efficiency of 6.05% with a maximum IPCE value of 65% at 540 nm. The data presented herein suggest that **YS5** is a truly promising sensitizer for nanocrystalline TiO_2-based DSSCs and appears poised for widespread adaptation.

Acknowledgment. This research was supported by the Air Force Office of Scientific Research (FA9550-05-1-0276), the State of Ohio (Wright Center for Photovoltaics Innovation and

Commercialization, PVIC), the National Science Foundation (CHE-0719050), and the Air Force Research Laboratory, Space Vehicles Directorate (AF9453-08-C-0172). The authors are indebted to Ms. Seung-Hung A. Lee and Prof. Thomas E. Mallouk of Pennsylvania State University for their initial assistance with the TiO_2 paste preparation and device assembly.

Supporting Information Available: ^{1}H NMR, ^{13}C NMR, ^{1}H−^{1}H COSY, HSQC, and HMBC spectra of **YS4**; electrochemistry of **YS5**; ATR-FTIR and resonance Raman spectra of **YS4** and **YS5** as neat solids and as adsorbed onto TiO_2 films along with Raman spectra of the TiO_2 nanoparticles (PDF). This material is available free of charge via the Internet at http://pubs.acs.org.

REFERENCES AND NOTES

(1) O'Regan, B.; Grätzel, M. *Nature* **1991**, *353*, 737–740.
(2) Nazeeruddin, M. K.; Kay, A.; Rodicio, I.; Humphry-Baker, R.; Muller, E.; Liska, P.; Vlachopoulos, N.; Grätzel, M. *J. Am. Chem. Soc.* **1993**, *115*, 6382–6390.
(3) Yu, G.; Gao, J.; Hummelen, J. C.; Wudl, F.; Heeger, A. J. *Science* **1995**, *270*, 1789–1791.
(4) Halls, J. J. M.; Walsh, C. A.; Greenham, N. C.; Marseglia, E. A.; Friend, R. H.; Moratti, S. C.; Holmes, A. B. *Nature* **1995**, *376*, 498–500.
(5) Cherepy, N. J.; Smesad, G. P.; Grätzel, M. *J. Phys. Chem. B* **1997**, *101*, 9342–9351.
(6) Bach, U.; Lupo, D.; Comte, P.; Moser, J. E.; Weissörtel, F.; Salbeck, J.; Spreitzer, H.; Grätzel, M. *Nature* **1998**, *395*, 583–585.
(7) Hagfeldt, A.; Grätzel, M. *Acc. Chem. Res.* **2000**, *33*, 269–277.
(8) McFarland, E. W.; Tang, J. *Nature* **2003**, *421*, 616–618.
(9) Yanagida, S. *C. R. Chim.* **2006**, *9*, 597–604.
(10) Hino, T.; Ogawa, Y.; Kuramoto, N. *Carbon* **2006**, *44*, 880–887.
(11) Staniszewski, A.; Ardo, S.; Sun, Y. L.; Castellano, F. N.; Meyer, G. J. *J. Am. Chem. Soc.* **2008**, *130*, 11586–11587.
(12) Ardo, S.; Sun, Y.; Staniszewski, A.; Castellano, F. N.; Meyer, G. J. *J. Am. Chem. Soc.* **2010**, *132*, 6696–6709.
(13) Grätzel, M. *J. Photochem. Photobiol., C* **2003**, *4*, 145–153.
(14) Bessho, T.; Yoneda, E.; Yum, J.; Guglielmi, M.; Tavernelli, I.; Imai, H.; Rothlisberger, U.; Nazeeruddin, M. K.; Grätzel, M. *J. Am. Chem. Soc.* **2009**, *131*, 5930–5934.
(15) Nazeeruddin, M. K.; Pechy, P.; Renouard, T.; Zakeeruddin, S. M.; Humphrey-Baker, R.; Comte, P.; Liska, P.; Cevey, L.; Costa, E.; Shklover, V.; Spiccia, L.; Deacon, G. B.; Bignozzi, C. A.; Grätzel, M. *J. Am. Chem. Soc.* **2001**, *123*, 1613–1624.
(16) Baruch, P. J. *J. Appl. Phys.* **1985**, *57*, 1347–1355.
(17) Wang, P.; Zakeeruddin, S. M.; Exnar, I.; Grätzel, M. *Chem. Commun.* **2002**, *24*, 2972–2973.
(18) Wang, P.; Zakeeruddin, S. M.; Comte, P.; Charvet, R.; Humphry-Baker, R.; Grätzel, M. *J. Phys. Chem. B* **2003**, *107*, 14336–14341.
(19) Wang, P.; Zakeeruddin, S. M.; Moser, J. E.; Humphry-Baker, R.; Comte, P.; Aranyos, V.; Hagfeldt, A.; Nazeeruddin, M. K.; Grätzel, M. *Adv. Mater.* **2004**, *16*, 1806–1812.
(20) Wang, P.; Klein, C.; Humphry-Baker, R.; Zakeeruddin, S. M.; Grätzel, M. *J. Am. Chem. Soc.* **2005**, *127*, 808–809.
(21) Klein, C.; Nazeeruddin, M. K.; Liska, P.; Censo, D. D.; Hirata, N.; Palomares, E.; Durrant, J. R.; Grätzel, M. *Inorg. Chem.* **2005**, *44*, 178–180.
(22) Gao, F.; Wang, Y.; Zhang, J.; Shi, D.; Wang, M.; Humphry-Baker, R.; Wang, P.; Zakeeruddin, S. M.; Grätzel, M. *Chem. Commun.* **2008**, *23*, 2635–2637.
(23) Grätzel, M. *Inorg. Chem.* **2005**, *44*, 6841–6851.
(24) Alford, P. C.; Cook, M. J.; Lewis, A. P.; McAuliffe, G. S. G.; Skarda, V.; Thomson, A. J.; Glasper, J. L.; Robbins, D. J. *J. Chem Soc., Perk. Trans. 2* **1985**, 705–709.
(25) Vierling, P.; Garelli, N. *J. Org. Chem.* **1992**, *57*, 3046–3051.
(26) Leadbeater, N. E.; Torenius, H. M.; Tye, H. *Tetrahedron* **2003**, *59*, 2253–2258.
(27) Wang, P.; Zakeeruddin, S. M.; Moser, J. E.; Nazeeruddin, M. K.; Sekiguchi, T.; Grätzel, M. *Nat. Mater.* **2003**, *2*, 402–407.
(28) Tyson, D. S.; Castellano, F. N. *J. Phys. Chem., A* **1999**, *103*, 10955–10960.
(29) Sawyer, D. T. S., A.; Roberts, J. L., Jr. *Electrochemistry for Chemists*, 2nd ed.; John Wiley & Sons: New York, 1995.
(30) Lee, S. H. A.; Abrams, N. M.; Hoertz, P. G.; Barber, G. D.; Halaoui, L. I.; Mallouk, T. E. *J. Phys. Chem. B* **2008**, *112*, 14415–14421.
(31) Onicha, A. C.; Castellano, F. N. *J. Phys. Chem. C* **2010**, *114*, 6831–6840.
(32) Chen, C. Y.; Wu, S. J.; Li, J. Y.; Wu, C. G.; Chen, J. G.; Ho, K. C. *Adv. Mater.* **2007**, *9*, 3888–3891.
(33) Choi, H.; Baik, C.; Kim, S.; Kang, M. S.; Xu, X.; Kang, H. S.; Kang, S. O.; Ko, J.; Nazeeruddin, M. K.; Grätzel, M. *New J. Chem.* **2008**, *32*, 2233–2237.
(34) Chen, C. Y.; Chen, J. G.; Wu, S. J.; Li, J. Y.; Wu, C. G.; Ho, K. C. *Angew. Chem.* **2008**, *120*, 7452–7455.
(35) Abbotto, A.; Barolo, C.; Bellotto, L.; De Angelis, F.; Grätzel, M.; Manfredi, N.; Marinzi, C.; Fantacci, S.; Yum, J. H.; Nazeeruddin, M. K. *Chem. Commun.* **2008**, *42*, 5318–5320.
(36) Gao, F.; Wang, Y.; Shi, D.; Zhang, J.; Wang, M.; Jing, X.; Humphry-Baker, R.; Wang, P.; Zakeeruddin, S. M.; Grätzel, M. *J. Am. Chem. Soc.* **2008**, *130*, 10720–10728.
(37) Cao, Y.; Bai, Y.; Yu, Q.; Cheng, Y.; Liu, S.; Shi, D.; Gao, F.; Wang, P. *J. Phys. Chem. C* **2009**, *113*, 6290–6297.
(38) Phifer, C. C.; McMillin, D. R. *Inorg. Chem.* **1986**, *25*, 1329–1333.
(39) Kalyanasundaram, K.; Nazeeruddin, M. K.; Grätzel, M.; Viscardi, G.; Savarino, P.; Barni, E. *Inorg. Chim. Acta* **1992**, *198*, 831–839.
(40) Cook, M. J.; Lewis, A. P.; McAuliffe, G. S. G.; Skarda, V.; Thomson, A. J. *J. Chem. Soc., Perk. Trans. 2* **1984**, *8*, 1293–1301.
(41) Lin, C.-T.; Böttcher, W.; Chou, M.; Creutz, C.; Sutin, N. *J. Am. Chem. Soc.* **1976**, *98*, 6536–6544.
(42) Nazeeruddin, M. K.; Zakeeruddin, S. M.; Humphry-Baker, R.; Jirousek, M.; Liska, P.; Vlachopoulos, N.; Shklover, V.; Fischer, C.-H.; Grätzel, M. *Inorg. Chem.* **1999**, *38*, 6298–6305.
(43) Yanagida, M.; Singh, L. P.; Sayama, K.; Hara, K.; Katoh, R.; Islam, A.; Sugihara, H.; Arakawa, H.; Mohammad, K. N. G., M. *J. Chem. Soc., Dalton Trans.* **2000**, *16*, 2817–2822.
(44) Anderson, N. A.; Lian, T. Q. *Annu. Rev. Phys. Chem.* **2005**, *56*, 491–519.
(45) Kallioinen, J.; Benko, G.; Sundstrom, V.; Korppi-Tommola, J. E. I.; Yartsev, A. P. *J. Phys. Chem. B* **2002**, *106*, 4396–4404.
(46) Hagfeldt, A.; Grätzel, M. *Chem. Rev.* **1995**, *95*, 49–68.
(47) Kalyanasundaram, K.; Grätzel, M. *Coord. Chem. Rev.* **1998**, *177*, 347–414.
(48) O'Regan, B. C.; Durrant, J. R. *Acc. Chem. Res.* **2009**, *42*, 1799–1808.
(49) Benko, G.; Skarman, B.; Wallenberg, R.; Hagfeldt, A.; Sundstrom, V.; Yartsev, A. P. *J. Phys. Chem. B* **2003**, *107*, 1370–1375.
(50) Wang, Z.-S.; Kawauchi, H.; Kashima, T.; Arakawa, H. *Coord. Chem. Rev.* **2004**, *248*, 1381–1389.
(51) Kao, M. C.; Chen, H. Z.; Young, S. L.; Kung, C. Y.; Lin, C. C. *Thin Solid Films* **2009**, *517*, 5096–5099.
(52) Kuang, D.; Brillet, J.; Chen, P.; Takata, M.; Uchida, S.; Miura, H.; Sumioka, K.; Zakeeruddin, S. M.; Grätzel, M. *ACS Nano* **2008**, *2*, 1113–11136.
(53) Tan, B.; Wu, Y. Y. *J. Phys. Chem. B* **2006**, *110*, 15932–15938.
(54) Huang, C. Y.; Hsu, Y. C.; Chen, J. G.; Suryanarayanan, V.; Lee, K. M.; Ho, K. C. *Sol. Energy Mater. Sol. Cells* **2006**, *90*, 2391–2397.
(55) Polo, A. S.; Itokazu, M. K.; Iha, N. Y. M. *Coord. Chem. Rev.* **2004**, *248*, 1343–1361.
(56) Boschloo, G.; Hagfeldt, A. *Acc. Chem. Res.* **2009**, *42*, 1819–1826.

AM100311M